Letters

Multifrequency Model of Sinusoidal PWM by DIDR Methodology

Tao Zhang, Hui Wang, Jingshuo Yan, Jiawen Wang, Enwei Zhang, Yifei Wang, and Bai Guo

***Abstract*—The multifrequency (MF) model of sinusoidal pulsewidth modulation can address unprecedented cross-frequency dynamics of ac/dc converters. Considering the small signal condition, it *corresponds to* the multiplication of the disturbed modulation signal and the unit impulse band sequence through *dimensionality increase, followed by dimensionality reduction methodology*. Cross-frequency gains introduced by switching and sideband frequency are evaluated through double Fourier coefficients of the sequence. Incorporating these effects, superior accuracy is achieved in time and frequency domains, facilitating dynamic stability analysis through the passivity method. The technique establishes a rigorous foundation for an MF model of converters, further for a dynamic analysis framework.**

***Index Terms*—Dimensionality increase followed by dimensionality reduction (DIDR) methodology, double Fourier series, multifrequency (MF) model, sinusoidal pulsewidth modulation.**

I. Introduction

INCREASING *penetration of power converters* with heterogeneous switching frequencies introduces complicated high-frequency interactions in the power system. Consequently, unexpected behaviors, such as beat frequency oscillation [1], *wideband resonance, and harmonic instability* [2], have emerged, posing significant challenges to dynamic analytical frameworks. Conventional analysis builds on a small-signal model focusing on single-frequency responses, failing to capture cross-frequency interactions. The multifrequency (MF) model of ac/dc converters provides a systematic solution to these dynamic challenges, which hinges on accurate MF representation of sinusoidal pulsewidth modulation (SPWM).

MF incorporates switching and sideband frequency of SPWM, in contrast to representing SPWM by a linear element, including a proportional amplifier [3], a time delayer [4], and a zero-order holder [5]. Based on linear description, literatures derive the impedance of ac/dc converter in stationary [3] and rotating frames [6], utilizing harmonic linearization and space vectors method respectively, providing foundational support for stability analysis [7]. However, these *linearized models* fail to capture *high-frequency interactions* and exhibit diminishing accuracy in the *high-frequency range* [8]. The *double Fourier series (DFS)* method offers the *multifrequency representation of modulation stages* [9], *which is developed* for pulsewidth modulation in communication systems [10]. It involves an elegant methodology manipulating converters with more than one independent frequency: *dimensionality increase followed by dimensionality reduction (DIDR).* This technique is adopted to represent *frequency spectra of various PWM waveforms* [11]. A 3-D metope with double periodicity is defined, and the *switching function* of SPWM (i.e., its output) is characterized by the intersection of the metope and a cylinder. Nevertheless, *double-periodicity of the metope breaks down* under perturbed conditions, rendering the method inadequate to snap multifrequency dynamics *of SPWM.* The authors in [12] and [13] break through the limitation by decomposing PWM into *three constituent components.* It enables model derivation via a *1-D Fourier series, which* is generalized for *multilevel converters* [14]. The applications are constrained by *complex representation* and *overmodulation-induced* degradation. Recent research in [15] explores the MF model *of SPWM* under the restrictive assumption of *integer carrier ratios.* It is *overly conservative* since *switching frequency* $\omega_{\rm sw}$ $(= 2\pi f_{sw})$ *and modulation frequency* $\omega_{\rm m}$ $(= 2\pi f_m)$ *are typically commensurable*.

This letter presents a novel MF model of SPWM, combining an elegant description of the *DFS method,* the applicability of the *1-D Fourier series method* under perturbed condition, and overcoming restrictive assumption of *integer carrier ratios*. MF corresponds to the multiplication of the disturbed modulation signal and the unit impulse band sequence. Cross-frequency gains are evaluated through double Fourier coefficients of the sequence. Model performance of ac/dc converters is improved by incorporating these gains, thus facilitating high-frequency stability analysis. Contributions of this letter include: 1) developing MF of SPWM with general carrier following by *DIDR methodology*; 2) validating superior accuracy in the time domain and precise stability assessment in the frequency domain through the passivity method; 3) discussing associations with common modulations. This letter establishes a rigorous

Received 9 June 2025; revised 1 August 2025; accepted 10 August 2025. Date of publication 13 August 2025; date of current version 22 October 2025. This work was supported in part by the Key Program of Joint Fund for Regional Innovative Development of the National Natural Science Foundation of China under Grant U23A20654 and in part by the National Natural Science Foundation of China under Grant 52177183. *(Corresponding author: Hui Wang.)*

Tao Zhang, Hui Wang, Jingshuo Yan, Jiawen Wang, and Enwei Zhang are with the School of Electrical Engineering, Shandong University, Jinan 250012, China (e-mail: 202014622@mail.sdu.edu.cn; sddlwh@sdu.edu.cn; yjs1120@njust.edu.cn; wangsus@mail.sdu.edu.cn; 202100190246@mail.sdu.edu.cn).

Yifei Wang is with State Grid Qinghai Electric Power Research Institute, Xining 810008, China (e-mail: 201834372@mail.sdu.edu.cn).

Bai Guo is with State Grid Laiwu Electric Power Company, Laiwu 250102, China (e-mail: 202034650@mail.sdu.edu.cn).

Color versions of one or more figures in this article are available at https://doi.org/10.1109/TPEL.2025.3598802.

Digital Object Identifier 10.1109/TPEL.2025.3598802

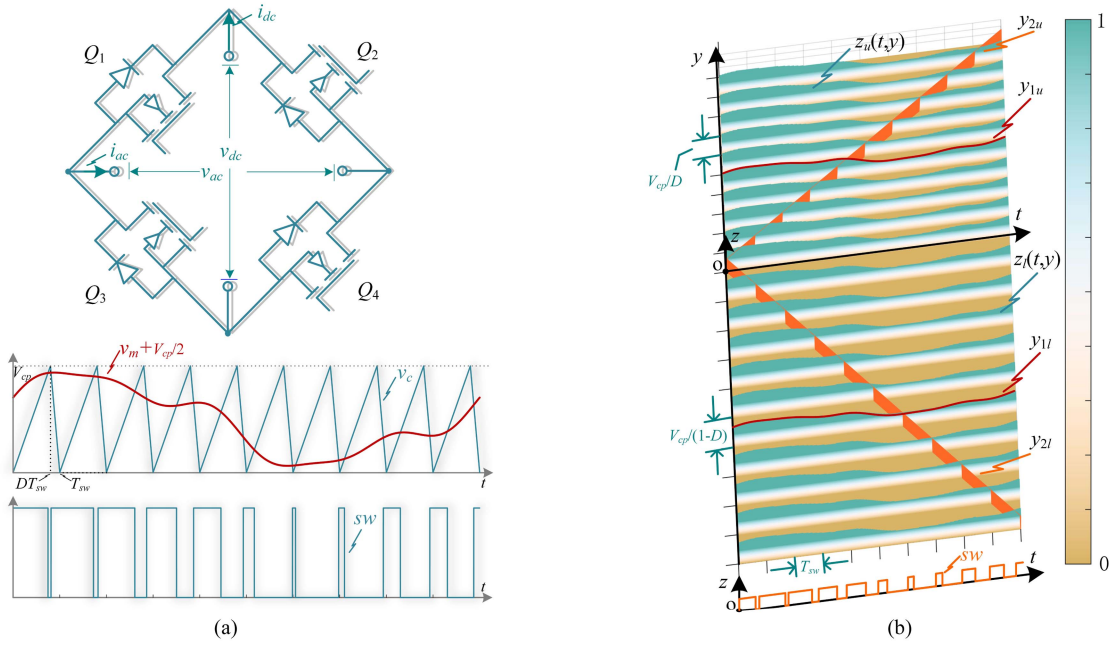

Fig. 1. Modulation principle of SPWM under 2-D and 3-Dsystem. (a) Two-dimensional system. (b) Three-dimensional system.

foundation for the unprecedented dynamic behaviors of ac/dc converters.

II. MF Model of SPWM

The switching function sw plays a fundamental role in constructing the MF of ac/dc converters. It is generated through the comparison between the modulation signal v_m and the carrier v_c.

Fig. 1(a) demonstrates this principle within a 2-D system, where the switching function's impact on the converter is illustrated employing an H-bridge topology. $v_{\rm ac}$, $v_{\rm dc}$, $i_{\rm ac}$, and $i_{\rm dc}$ describe ac voltage, dc voltage, ac current, and dc current, respectively. H-bridge's operation under bipolar modulation strategy is characterized by

$$\begin{bmatrix} v_{\rm ac} \\ i_{\rm dc} \end{bmatrix} = \begin{bmatrix} 2sw-1 & 0 \\ 0 & 2sw-1 \end{bmatrix} \begin{bmatrix} v_{\rm dc} \\ i_{\rm ac} \end{bmatrix}. \tag{1}$$

The general carrier waveform in Fig. 1(a) is described in

$$v_c = \frac{V_{cp}}{T_{sw}} \begin{cases} \frac{t-kT_{sw}}{D}, t \in (kT_{sw}, (k+D)T_{sw}] \\ -\frac{t-(k+1)T_{sw}}{1-D}, t \in ((k+D)T_{sw}, (k+1)T_{sw}] \end{cases} \tag{2}$$

where k (= 01,2 …) defines the kth switching period, while V_{cp}, T_{sw}, and D denote the carrier's peak-to-peak value, switching period, and duty cycle of the rising slope, respectively. Transitions of switching function depend on the intersection between v_m+V_{cp}/2 and v_c, which is equivalently expressed in

$$\begin{cases} v_m + \frac{V_{cp}}{2} + \frac{kV_{cp}}{D} = \frac{V_{cp}}{DT_{sw}} t, t \in (kT_{sw}, (k+D)T_{sw}] \\ v_m + \frac{V_{cp}}{2} - \frac{(k+1)V_{cp}}{1-D} = \frac{-V_{cp}}{(1-D)T_{sw}} t, t \in ((k+D)T_{sw}, (k+1)T_{sw}]. \end{cases} \tag{3}$$

For analytical tractability, reformulate both sides of (3) as

$$\begin{cases} y_{1u} = v_m + \frac{V_{cp}}{2} + \frac{kV_{cp}}{D}, y_{2u} = \frac{V_{cp}}{DT_{sw}} t \\ y_{1l} = v_m + \frac{V_{cp}}{2} - \frac{(k+1)V_{cp}}{1-D}, y_{2l} = \frac{-V_{cp}}{(1-D)T_{sw}} t \end{cases} \tag{4}$$

in which the unary temporal functions y_{1x} ($x = u,l$) and y_{2x} denote the curve families determined by modulation signal, and ramp functions associated with both carrier slopes, respectively. The subscript u (l) indicates the upper (lower) half-plane of the 2-D system, given that k is a nonnegative integer. The switching condition is transformed to the intersections between y_{1x} and y_{2x}. While it appears similar to the fundamental principle of SPWM, an elegant phenomenon occurs under the direction of DIDR methodology. Fig. 1(b) introduces axis z perpendicular to the original toy plane, establishing a 3-D system that incorporates an independent temporal axis t, spatial dimension y, and functional dimension z. The metopes $z_x(t,y)$ enveloped by y_{1x} are constructed in this system with their height encoded by the color bar. The crosslines are generated when orange cylinders spanned by y_{2x} cross over the metopes, which are mapped onto the toz plane to retrieve the switching function. Therefore, sw is mathematically recovered by substituting y_{2x} into $z_x(t,y)$

$$sw = z_u\left(t, y_{2u}\right) + z_l\left(t, y_{2l}\right) \tag{5}$$

reducing the system dimensionality back to two. Notably, $z_x(t,y)$ means the binary function in 3-D system, whereas $z_x(t,y_{2x})$, the unary temporal function, describes the projection of crosslines onto toz plane. A critical observation is that (5) remains valid under perturbed conditions. The small-signal component of the switching function Δsw is derived accordingly as

$$\Delta sw = \Delta z_u\left(t, y_{2u}\right) + \Delta z_l\left(t, y_{2l}\right) \tag{6}$$

where $\Delta z_x(t,y_{2x})$, small-signal perturbation of the projection, is intractable to obtain directly. Instead, it can be derived through the analysis of the binary function $\Delta z_x(t,y)$ foremost.

Consider an arbitrary coordinate pair (t,y) satisfying the steady-state curves family Y_{1x}. A rectangular pulse with an area quantity of Δv_m appears at this location when the modulation signal is subject to a small-signal disturbance. Applying the equal area principle, the pulse can be represented by the multiplication of Δv_m and a Dirac function. Extending the above analysis to the entire toy plane yields an impulse band sequence

$$\Delta z_x(t,y) = \Delta v_m \delta\left(t, Y_{1x}\right) \tag{7}$$

where $\delta(t,Y_{1x})$ denote unit impulse band sequences with spatial characteristics satisfying the expressions of Y_{1x}. The sequences exhibit double periodicity: T_m-periodicity along axis t, and V_{cp}/D_x-periodicity in dimension y. D_x indicates the duty cycle of the corresponding carrier slope ($D_x = D$ for $x = u$, and D_x= 1-D for $x = l$). Therefore, it can be expanded to its DFS shown in

$$\begin{cases} \delta(t,Y_{1x}) = \sum_{p=-\infty}^{+\infty}\sum_{q=-\infty}^{+\infty} \Lambda_{p,q}^{x} e^{j(p\omega_m t + q\frac{2D_x\pi}{V_{cp}}y)} \\ \Lambda_{p,q}^{x} = \frac{D_x e^{-jqD_x\pi}}{T_m V_{cp}} \int_0^{T_m} e^{-j(p\omega_m t + q\frac{2D_x\pi}{V_{cp}}V_m)} \mathrm{d}t \end{cases} \tag{8}$$

where $\Lambda_{p,q}^{x}$ symbolize double Fourier coefficients. Substituting (8) into (7), then replacing y with y_{2x} arrives at

$$\Delta z_x\left(t, y_{2x}\right) = \Delta v_m \sum_{p=-\infty}^{+\infty}\sum_{q=-\infty}^{+\infty} \Lambda_{p,q}^{x} e^{j(p\omega_m + c_x q\omega_{sw})t} \tag{9}$$

in which $c_x = 1$ for $x = u$, and $c_x = -1$ for $x = l$. Combination of (6) and (9) yields

$$\Delta sw = \Delta v_m \sum_{p=-\infty}^{+\infty}\sum_{q=-\infty}^{+\infty} \left(\Lambda_{p,q}^{u} + \Lambda_{p,-q}^{l}\right) e^{j(p\omega_m + q\omega_{sw})t}. \tag{10}$$

The analytical formulation demonstrates that the disturbed switching function is represented by the multiplication of the disturbed modulation signal and a DFS. The composite coefficients $\Lambda_{p,q}^{u} + \Lambda_{p,-q}^{l}$ quantify the cross-frequency gains inherent in SPWM. These can be computed numerically for any specified modulation signal V_m and any given carrier form. In particular, the cross-frequency gains are exclusively described by $\Lambda_{p,q}^{u}$ or $\Lambda_{p,-q}^{l}$, respectively, if a trailing edge carrier or a leading edge carrier is employed in modulation. Notice from (8) that the 0th order coefficient $\Lambda_{0,0}^{u} + \Lambda_{0,0}^{l}$ becomes equal to the reciprocal of the carrier's peak-to-peak value. This illustrates why SPWM is simplified as an amplifier in conventional modeling analysis. The workflow to obtain MF of SPWM gets around an integer carrier ratio, thereby establishing a universal modeling framework.

Supposing V_m is characterized by

$$V_m = \sum_k V_{mk} \sin\left(k\omega_m t + \varphi_k\right) \tag{11}$$

where V_{mk} and φ_k represent the magnitude and phase at multiples of modulation frequency $k\omega_m$. Analytical solution of cross-frequency gains is accessible in (12) when V_m is exclusively composed of the ω_m component

$$\Lambda_{p,q}^{x} = (-1)^p D_x e^{jp\varphi_1} e^{-jqD_x\pi} J_p(qMD_x\pi)/V_{cp}. \tag{12}$$

$M = V_{m1}/(V_{cp}/2)$ signifies the modulation ratio, and $J_p(\bullet)$ denotes the pth order Bessel function of the first kind.

III. Model Verification

Comprehensive verification is conducted based on single-phase inverters (SPI). The inverters are composed of the H-bridge topology, filter networks, and a passive load/power grid. SPWM with 50-Hz modulation frequency is implemented digitally. In total, a 20-kHz sampling frequency of analog-to-digital conversion (ADC) is adopted to achieve a compromise between computational power and control resolution. The switching frequency is chosen as 888 Hz to satisfy the following requirements: 1) getting around the integer carrier ratio, and 2) feasibility to approximate digital modulation as an analog counterpart. Control delay and *images* induced by ADC are negligible given the parameters since sampling frequency is far outweighing switching frequency. It facilitates the specialized investigation of SPWM on stability, complying with the workflow in [5]. The validation encompasses two cases: 1) time domain state responses comparisons under open loop mode, and 2) frequency domain admittance derivation followed by passivity-based stability assessment under current mode.

A. Validation Case1: State Responses of Open-Loop Mode SPI

Case1 is conducted with the inverter depicted in Fig. 2(a). It is powered by a 50 V dc source V_{in}, through L_{dc} (= 2.6 mH) and C_{dc} (= 5 mF). Its output feeds a combination of resistor R (= 4.9 Ω) and saturable inductor L_f (flux–current curve shown in the figure). Two modeling approaches of the H-bridge are employed for comparative analysis. The switching-device-based model (SDBM) serves as the control group, where *sw* is generated through the comparison between the modulation signal and the carrier signal. The model retrieved from cross-frequency gains (MRMG) is taken as the experimental group, in which the H-bridge is represented by controlled sources governed by (1). *sw* is synthesized through the superposition of Δsw and *SW* (i.e., the steady state switching function). Δsw is approximated by the truncated spectral representation of (10). The modulation stage with a trailing edge carrier is implemented by the enhanced PWM module of the digital signal processor. The 150/8 MHz time-base clock determines that the carrier's peak-to-peak value equals 21115. V_m incorporates ω_m, $3\omega_m$, and $5\omega_m$ components with respective magnitudes of [0.8, 0.2, 0.1]×V_{cp} /2 and phase of [π/6, -π/12, π/5].

Given the inverter configuration, cross-frequency gains $\Lambda_{p,q}$, and the sum of $\Lambda_{p,q}^{u}$ and $\Lambda_{p,-q}^{l}$, are derived from (8) and visualized in Fig. 2(b). The contributions from high-order cross-frequency gains are nonnegligible. When a perturbation at frequency ω_p is introduced to the modulation signal, the switching function exhibits characteristic spectral components at frequency $p\omega_m$+$q\omega_{sw}$+ω_p. Null values of $\Lambda_{p,0}$ prevent the interactions between perturbation and modulation frequency.

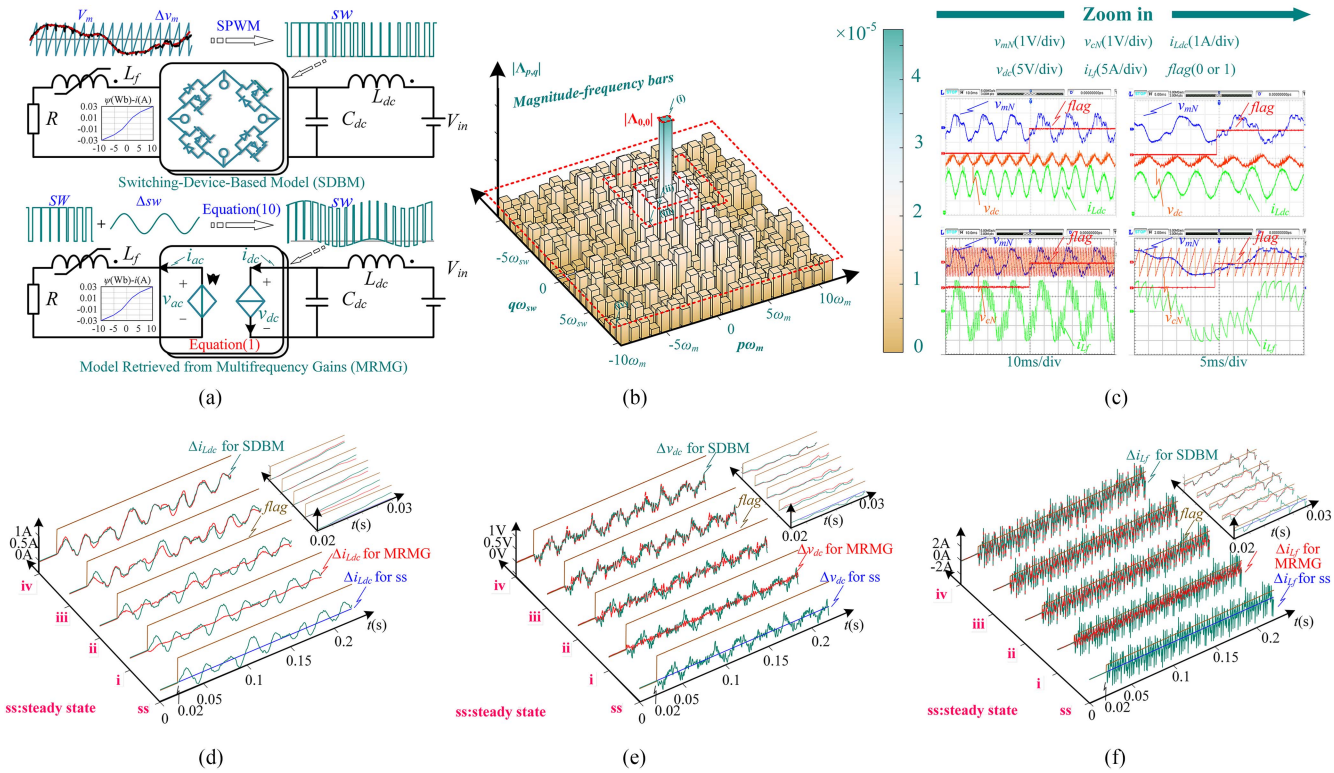

Fig. 2. Model employment, cross-frequency gains from SPWM, experimental waveforms, and model comparisons. (a) Deployment of model for validation. (b) Cross-frequency gains from SPWM. (c) Experimental waveforms. (d) Comparisons in terms of Δi_{Ldc}. (e) Comparisons in terms of Δv_{dc}. (f) Comparisons in terms of Δi_{Lf}.

For low-frequency perturbations ($\omega_p << \omega_{sw}/2$), switching ($q\omega_{sw}+\omega_p$) and sideband components ($p\omega_m + q\omega_{sw} + \omega_p$) appear in high-frequency bands, thus effectively attenuated by the low-pass characteristics. The perturbations of state variables are dominated by the ω_p component, allowing SPWM to function as a linear amplifier. The spectral redistribution emerges as ω_p increases: the perturbation component migrates to higher frequency, while the associated switching/sideband component appears in the lower frequency band. The influence of switching/sideband components on state variables is progressively enhanced. Consequently, the linear amplifier approximation becomes inaccurate, particularly in the high-frequency range. To maintain modeling fidelity across the entire frequency range, explicit incorporation of switching/sideband components is essential for capturing cross-frequency dynamics.

Correlation coefficient (COV) between SDBM and MRMG, as well as Euclidean norm (Norm) of the model errors, are introduced to describe the discrepancy with respect to the truncation numbers of 0, 1, 3, 5, and 11. Truncation numbers correspond to steady state and four distinct regions enclosed by dotted lines (i), (ii), (iii), and (iv) in Fig. 2(b), respectively. A 500-Hz square wave with $\pm V_{cp}$ /20 magnitude is injected. The waveforms of state variables, including current $i_{L\mathrm{dc}}$ through L_{dc}, current i_{Lf} through L_f, and voltage v_{dc} across C_{dc}, are derived experimentally as Fig. 2(c). v_{mN} ($= 2v_m/V_{cp}$) and v_{cN} ($= 2v_c/V_{cp}$) denote normalized modulation signal and carrier, and *flag* designates whether perturbation has been injected. The comparison results have been summarized in Fig. 2(d)–(f). These 3-D plots illustrate the temporal evolution of state variables' perturbation components following a perturbation at $t = 0.02$ s. The truncation numbers are mapped onto an independent axis, with the corresponding [COV, Norm] pairs annotated at the bottom of the diagram. Notice that COV and Norm approach 1 and 0, respectively, with the increase of the truncation number. SDBM tends to coincide with MRMG of higher truncation number, which means the achievement of a more precise model if cross-frequency gains are incorporated.

B. Validation Case2: Admittance and Stability Analysis of Current Mode SPI

To clarify the significance of SPWM in highly precise modeling of ac/dc converters and stability assessment, a grid-connected SPI and its control block diagram are presented in Fig. 3(a). It comprises a 200-V dc source, converter-side inductance L ($= 5.2$ mH), damping resistor R ($= 0.2\ \Omega$ except where noted), grid-side capacitance C_g ($= 5\ \mu$F except where noted), and inductance L_g ($= 1.5$ mH). An infinite ac power supply V_g is connected with this inverter, and the synchronization between them is through the symmetrical PLL proposed in [16]. The dynamic of PLL is omitted in subsequent analysis for its bandwidth limitation above the Nyquist frequency.

Without loss of generality, PR controller $G_c(s)$ is applied to regulate converter-side current i_c at amplitude $I_m = 10$ A with unit power factor, where k_p ($= 400$) and k_r ($= 35\ 000$) denote

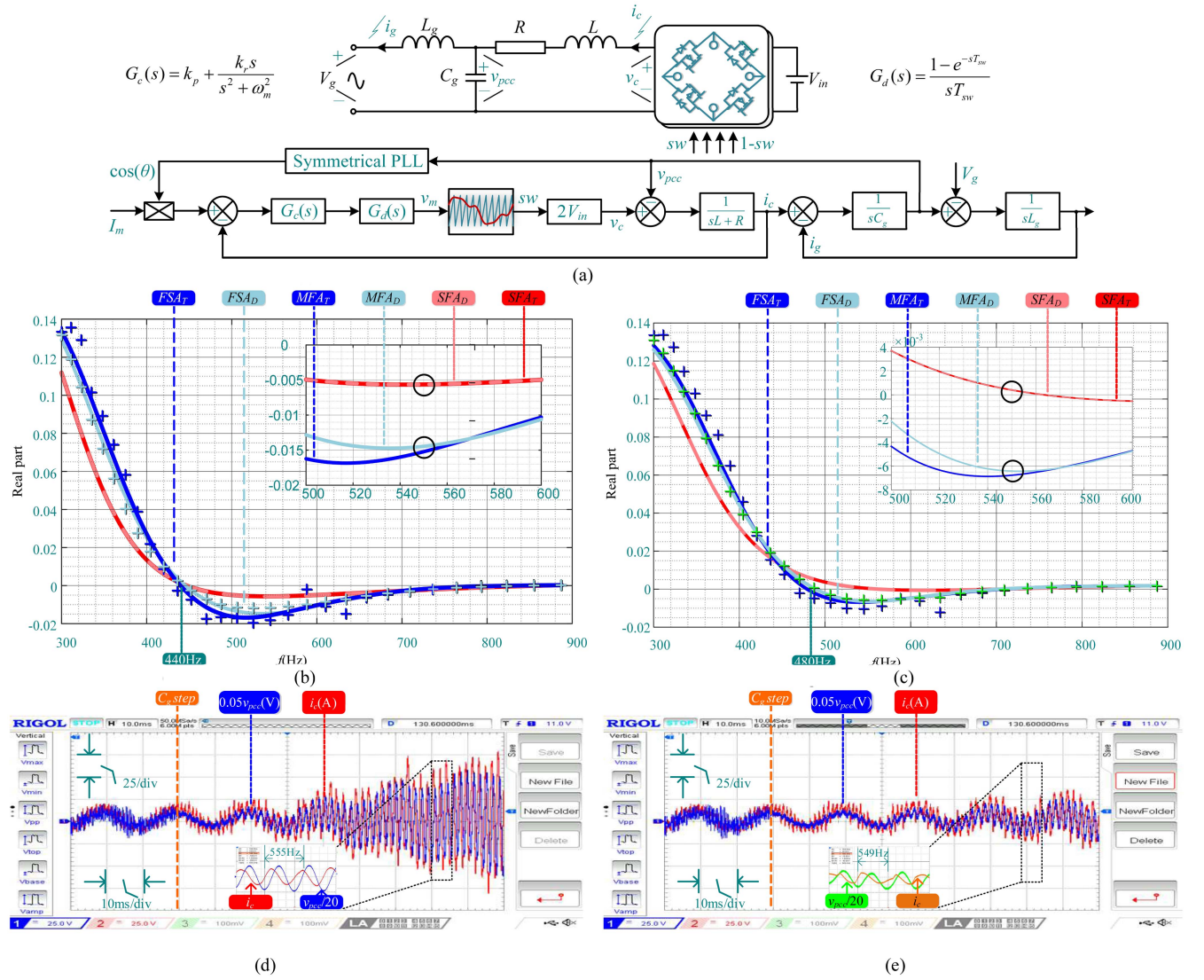

Fig. 3. Topology of single-phase inverter, comparisons in real part of admittance and time domain waveforms. (a) Topology of grid connected single phase inverter and its control block diagram. (b) Real part of admittance under $R = 0.2\ \Omega$. (c) Real part of admittance under $R = 1.5\ \Omega$. (d) Time domains waveform under $R = 0.2\ \Omega$. (e) Time domain waveforms under $R = 1.5\ \Omega$.

corresponding gains. Notice that the sampling effect from ADC and the delay introduced by the control in [5] are not depicted in the block diagram of Fig. 3(a) since sampling frequency significantly exceeds switching frequency. The passivity of SISO admittance $Y_{\text{in}}(s)$ is accordingly explicit in the high-frequency range, mitigating potential instability risks. To come up to the surface effect of the modulation stage on admittance and facilitate subsequent stability analysis, a zero-order holder $G_d(s)$ is deliberately incorporated into the control loop. Conventional SPWM model-based single-frequency admittance, presented model-based MF admittance, frequency sweeping results with MATLAB, and corresponding time domain waveforms from experiment are obtained to facilitate the analysis. The theoretical derivations for single-frequency or MF admittance comply with the same workflow as that in [5].

Given the above validation configurations, the real part of the admittance within the range of 300 Hz–1 kHz is presented in Fig. 3(b) and (c). The visual representation employs specification: 1) heavy/light red lines represent the single-frequency admittance with trailing edge/double edge carrier SPWM (SFA_T/SFA_D), 2) heavy/light blue lines depict corresponding MF admittance (MFA_T/MFA_D) incorporating additional cross-frequency effects induced by $\pm f_{sw} \pm f_m$ (conclusion in [15]), and 3) heavy/light blue data markers characterize the relevant frequency sweeping results (FSA_T/FSA_D). It is observed that the following holds.

1) The single-frequency admittance is carrier-independent in high-frequency range, while MF admittance exhibits discrepancy when employing different carrier types.

2) The frequency-sweeping result shows stronger alignment with MF admittance, indicating the enhanced model accuracy in high-frequency range when considering the cross-frequency effect of SPWM.
3) Single-frequency admittance yields conservative passivity assessment compared with MF admittance, which may result in the instability misjudgment. Further demonstration is conducted in the following.

As shown in Fig. 3(b), the weak damping system is subject to instability if the natural resonant frequency falls into the range 440 Hz–1000 Hz according to both single-frequency and MF admittance. Raising C_g from 5 to 72 μF yields a natural resonance mode at 550 Hz. Oscillation with this frequency occurs in the waveform of v_{pcc} and i_c under $R = 0.5\ \Omega$, as depicted in Fig. 3(d). This illustrates that both admittance models can precisely analyze system stability. The stability misjudgment using single-frequency admittance appears when system damping is enhanced through increasing R to 1.5 Ω. Given this condition, the real part of the single-frequency admittance at 550 Hz is positive, as shown in Fig. 3(c), indicating the passivity. However, the negative real part of the MF admittance at this resonance frequency provides the opposite conclusion. The divergent oscillations with a frequency of 550 Hz in Fig. 3(e) demonstrate the limitation of single-frequency admittance, which originates from the ignorance of cross-frequency gains of SPWM.

IV. Discussion

This letter indicates an easily overlooked yet important phenomenon that carrier types may influence high-frequency stability, which deserves further investigations. In addition, several critical viewpoints are discussed in the following.

A. Viewpoint1: Association With Other Modulation Stages

A fundamental signal named the switching function describes the switching dynamics in converters. It is generated through modulation stages, including SPWM, PWM, diode modulation (DM), and pulse frequency modulation (PFM). These are usually treated as an amplifier without cross-frequency effects incorporated, which deteriorates modeling accuracy in the high-frequency range particularly.

This letter demonstrates that the switching function of SPWM is represented by the multiplication of the disturbed modulation signal and the unit impulse band sequence. Note that this multiplicative form remains effective for other modulations. Specifically, the MF model of PWM and cross-frequency gains can be derived from (8) and (10) by replacing ω_m by ω_{sw} since modulation frequency is consistent with switching frequency. DM is, in essence, a comparator with the through current serving as the modulation signal. It is equivalent to SPWM with infinite peak-to-peak value and higher order infinite carrier period. Its MF model can be established by complying with the workflow outlined in (7)–(10). The distinction lies in the fact that the unit impulse band sequence has only one branch for its infinite period in the y dimension. Cross-frequency gains derivation demands a double Fourier transformation and its inverse operation. While (8) and (10) are not directly applicable for PFM, an alternative characterization is developed beginning with (5). The double periodicity enables DFS representation of steady-state metope $Z_x(t,y)$. The disturbed switching function can be retrieved by applying the first-order Taylor approximation on $Z_x(t,y_{2x})$.

B. Viewpoint2: Issues in MF Workflow and Relevant Solution

The periodicity of unit impulse band sequences $\delta(t,Y_{1x})$ is valid when V_m contains a dominant modulation frequency component. In validation Case1, the switching dependent components are attenuated by the low-pass filter effect of the zero-order holder, facilitating the application of (8) and (10). Generally speaking, feedback control transforms the modulation signal into a double periodic variable that invalidates DFS analysis. The limitation is resolved through a hybrid Fourier approach combining Fourier series decomposition in dimension y and Fourier transformation along the axis t. It enables precise characterization of cross-frequency gains, maintaining sufficient compatibility with the DIDR methodology.

Building on the derived MF model of modulation stages, a unified systematic workflow of converters can be knocked together to enhance the existing dynamic framework. It follows 1) *construction of a state space model, 2) determination of small signal model and steady state solution, 3) MF development for modulation stages, and 4) extraction of relevant transfer gains.* Furthermore, this workflow remains applicable for ac/ac converters with three independent frequencies.

MF of the dc/dc converter complying with the systematic workflow exhibits the form of a harmonic state space. The interested frequency components are structured as vectors, and the cross-frequency gains are arranged in matrices. MF of ac/dc converter in [17] remains this mathematical layout, resulting in significant issues regarding inflexible extensibility when accounting for harmonic truncation effects. The authors introduce an innovative mathematical architecture to address the constraint: interested frequency components are organized as matrices, and cross-frequency gains are arranged in tensors. The advanced representation employs the Einstein summation convention for all matrix-tensor operations, where repeated indices sum over.

V. Conclusion

In this letter, the MF model of SPWM is presented with the DIDR methodology. The disturbed switching function is represented by the multiplication of the disturbed modulation signal and the unit impulse band sequence. Cross-frequency gains are represented by double Fourier coefficients of the sequence. Superior accuracy is achieved by incorporating additional cross-frequency gains, facilitating unexpected dynamic analysis, particularly for stability assessment in the high-frequency range. The DIDR methodology reveals the fundamental associations between various modulation stages, offering transformative potential for reconstructing the dynamic analytical framework of power converters in the future.

REFERENCES

[1] X. Yue, D. Boroyevich, F. C. Lee, F. Chen, R. Burgos, and F. Zhuo, "Beat frequency oscillation analysis for power electronic converters in DC nanogrid based on crossed frequency output impedance matrix model," *IEEE Trans. Power Electron.*, vol. 33, no. 4, pp. 3052–3064, Apr. 2018.

[2] X. Wang and F. Blaabjerg, "Harmonic stability in power electronic-based power systems: Concept, modeling, and analysis," *IEEE Trans. Smart Grid*, vol. 10, no. 3, pp. 2858–2870, May 2019.

[3] M. Cespedes and J. Sun, "Impedance modeling and analysis of grid-connected voltage-source converters," *IEEE Trans. Power Electron.*, vol. 29, no. 3, pp. 1254–1261, Mar. 2014.

[4] L. Harnefors, X. Wang, A. G. Yepes, and F. Blaabjerg, "Passivity-based stability assessment of grid-connected VSCs—An overview," *IEEE J. Emerg. Sel. Topics Power Electron.*, vol. 4, no. 1, pp. 116–125, Mar. 2016.

[5] L. Harnefors, R. Finger, X. Wang, H. Bai, and F. Blaabjerg, "VSC input-admittance modeling and analysis above the nyquist frequency for passivity-based stability assessment," *IEEE Trans. Ind. Electron.*, vol. 64, no. 8, pp. 6362–6370, Aug. 2017.

[6] X. Wang, L. Harnefors, and F. Blaabjerg, "Unified impedance model of grid-connected voltage-source converters," *IEEE Trans. Power Electron.*, vol. 33, no. 2, pp. 1775–1787, Feb. 2018.

[7] J. Sun, "Impedance-based stability criterion for grid-connected inverters," *IEEE Trans. Power Electron.*, vol. 26, no. 11, pp. 3075–3078, Nov. 2011.

[8] C. Zhang, M. Molinas, S. Føyen, J. A. Suul, and T. Isobe, "Harmonic-domain SISO equivalent impedance modeling and stability analysis of a single-phase grid-connected VSC," *IEEE Trans. Power Electron.*, vol. 35, no. 9, pp. 9770–9783, Sep. 2020.

[9] H. Black, *Modulation Theory*. New York, NY, USA: Van Nostrand, 1953.

[10] W. R. Bennett, "New results in the calculation of modulation products," *Bell Syst. Tech. J.*, vol. 12, pp. 238–243, Apr. 1933.

[11] M. Sanchez and F. Popert, "Uber die berechrung der spektren modulierter impulsfolgen," *Arch. Elecktra Ubertrag*, vol. 9, pp. 441–452, Oct. 1955.

[12] H. Mouton and B. Putzeys, "Understanding the PWM nonlinearity: Single-sided modulation," *IEEE Trans. Power Electron.*, vol. 27, no. 4, pp. 2116–2128, Apr. 2012.

[13] H. T. Mouton, B. McGrath, D. G. Holmes, and R. H. Wilkinson, "One-dimensional spectral analysis of complex PWM waveforms using superposition," *IEEE Trans. Power Electron.*, vol. 29, no. 12, pp. 6762–6778, Dec. 2014.

[14] B. McGrath and H. T. Mouton, "One-dimensional spectral analysis techniques for multilevel PWM strategies," *IEEE Trans. Power Electron.*, vol. 31, no. 10, pp. 6910–6919, Oct. 2016.

[15] Y. Jiang, Y. Sun, J. Lin, S. Xie, and M. Su, "Multifrequency small-signal model for single-phase grid-tied inverters considering the effect of PWM," *IEEE Trans. Power Electron.*, vol. 39, no. 2, pp. 2128–2139, Feb. 2024.

[16] D. Yang, X. Wang, F. Liu, K. Xin, Y. Liu, and F. Blaabjerg, "Symmetrical PLL for SISO impedance modeling and enhanced stability in weak grids," *IEEE Trans. Power Electron.*, vol. 35, no. 2, pp. 1473–1483, Feb. 2020.

[17] K. J. P. Veeramraju, J. A. Mueller, and J. W. Kimball, "An extended generalized average modeling framework for power converters," *IEEE Trans. Power Electron.*, vol. 38, no. 8, pp. 9581–9592, Aug. 2023.